

Hybrid Graphene and Graphitic Carbon Nitride Nanocomposite: Gap Opening, Electron–Hole Puddle, Interfacial Charge Transfer, and Enhanced Visible Light Response

Aijun Du,^{*,†} Stefano Sanvito,[‡] Zhen Li,[§] Dawei Wang,[§] Yan Jiao,[†] Ting Liao,[†] Qiao Sun,[†] Yun Hau Ng,[⊥] Zhonghua Zhu,^{||} Rose Amal,[⊥] and Sean C. Smith[¶]

[†]Centre for Computational Molecular Science, Australian Institute for Bioengineering and Nanotechnology (AIBN), The University of Queensland, Queensland 4072, Brisbane, Australia

[‡]School of Physics and CRANN, Trinity College, Dublin 2, Ireland

[§]ARC Centre of Excellence for Functional Nanomaterials, Australian Institute for Bioengineering and Nanotechnology (AIBN), The University of Queensland, Queensland 4072, Brisbane, Australia

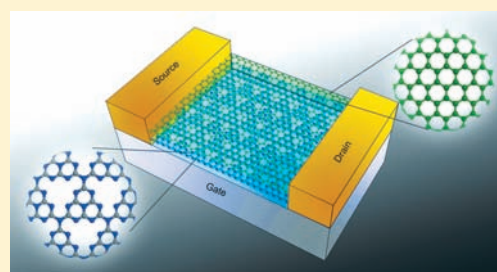
[⊥]ARC Centre of Excellence for Functional Nanomaterials, School of Chemical Sciences and Engineering, University of New South Wales, Sydney, New South Wales 2052, Australia

^{||}School of Chemical Engineering, University of Queensland, Queensland 4072, Brisbane, Australia

[¶]Centre for Nanophase Materials Sciences, Oak Ridge National Laboratory, Oak Ridge, Tennessee 37831, United States

Supporting Information

ABSTRACT: Opening up a band gap and finding a suitable substrate material are two big challenges for building graphene-based nanodevices. Using state-of-the-art hybrid density functional theory incorporating long-range dispersion corrections, we investigate the interface between optically active graphitic carbon nitride (g-C₃N₄) and electronically active graphene. We find an inhomogeneous planar substrate (g-C₃N₄) promotes electron-rich and hole-rich regions, i.e., forming a well-defined electron–hole puddle, on the supported graphene layer. The composite displays significant charge transfer from graphene to the g-C₃N₄ substrate, which alters the electronic properties of both components. In particular, the strong electronic coupling at the graphene/g-C₃N₄ interface opens a 70 meV gap in g-C₃N₄-supported graphene, a feature that can potentially allow overcoming the graphene's band gap hurdle in constructing field effect transistors. Additionally, the 2-D planar structure of g-C₃N₄ is free of dangling bonds, providing an ideal substrate for graphene to sit on. Furthermore, when compared to a pure g-C₃N₄ monolayer, the hybrid graphene/g-C₃N₄ complex displays an enhanced optical absorption in the visible region, a promising feature for novel photovoltaic and photocatalytic applications.



INTRODUCTION

Successful exfoliation of single layers of graphite, i.e., single-layer graphene,^{1,2} has opened up new exciting possibilities for development of the next generation of nanoelectronic devices. These are fueled by graphene's unique electronic structure^{3,4} and in particular by its extremely high charge carrier mobility. However, the lack of an intrinsic band gap implies that the current can never be turned off completely, i.e., a potential graphene-based field effect transistor (FET) is expected to show only modest on–off ratios.⁵ This has constituted a formidable hurdle to the use of graphene in logic and high-speed switching devices.^{6,7} To date, several strategies have been proposed for opening a band gap in graphene.^{8–13} These include cutting of 2D graphene into finite sized 1D nanoribbons,^{8,9} application of uniaxial strain,^{10,11} control of the patterned hydrogenation,¹² introduction of porosity,¹³ growth of epitaxial graphene on substrates,¹⁴ and use of molecule doping.¹⁵ Additionally, a band gap can be opened in Bernal-

stacked bilayer graphene by applying an external electric field normal to the graphene plane.^{16,17} However, despite these intensive research efforts, experimental realization of such schemes still remains a significant challenge.⁷

Another important challenge for development of graphene-based electronics is that devices made from a graphene monolayer should be supported on an ideal substrate.¹⁸ Graphene is very sensitive to its environment, and its remarkable high electron mobility can be affected by nearby materials. Thus, it is critical to finding the best substrate on which to mount graphene for more practical application. Currently, typical graphene-based devices are fabricated on either a SiO₂¹⁹ or a SiC substrate.²⁰ However, none of them is an ideal substrate for supporting graphene because of the highly rough substrate surface²¹ and the surface optical phonons.²²

Received: December 13, 2011

Published: February 16, 2012

Recently, growth of graphene on hexagonal boron nitride (BN) provides a potential solution to overcome such a challenge,^{18,23} although the effectiveness of the substrate depends strongly on the stacking order between BN and graphene.²⁴

Graphitic carbon nitride (g-C₃N₄) is a stacked two-dimensional structure, i.e., an analogue of graphite with N-substitution.²⁵ Recently, g-C₃N₄ has been demonstrated to be a potential candidate for optoelectronic conversion²⁶ and also a photocatalyst for water splitting into hydrogen.²⁷ However, the photoconversion efficiency in the visible range is rather low since the material shows only marginal absorption in that part of the spectrum.²⁵ As such, the optical absorption activity of g-C₃N₄ needs to be greatly improved before the materials become useful for photocatalysis. Experimentally, a hybrid graphene/g-C₃N₄ nanocomposite has been already successfully synthesized,²⁸ showing an enhanced photocatalytic activity upon visible light irradiation. However, the underlying mechanism for such an improvement remains unclear, and the interfacial electronic structure of the composite is completely unexplored.

The purpose of this study is to unveil whether or not there is strong electron coupling at the interface between electronically active graphene and optically active g-C₃N₄ materials. Particular attention will be focused on the following questions: (i) Is there a significant charge transfer between graphene and a g-C₃N₄ monolayer? (ii) Will a gap be opened in the gapless graphene if it is interfaced with the semiconducting g-C₃N₄? (iii) Can the optical properties of g-C₃N₄ be improved in the hybrid graphene/g-C₃N₄ complex as compared to those of a pure g-C₃N₄ monolayer?

In this article, hybrid functional calculations using the HSE06 functional²⁹ and including long-range dispersion corrections³⁰ have been carried out to accurately predict the structural and electronic properties of the hybrid graphene/g-C₃N₄ nanocomposite. We demonstrate, for the first time, that the graphene/g-C₃N₄ interface displays strong interlayer electron coupling. Most interestingly, a gap is opened for a g-C₃N₄-supported graphene layer, potentially overcoming the graphene band gap problem. Furthermore, the optical absorption spectrum of g-C₃N₄ shows the enhanced visible light response in the presence of graphene. Our results thus suggest the graphene/g-C₃N₄ composite can be used both as an electronic material for ultrafast electronics and as a photocatalyst for energy applications.

COMPUTATIONAL METHODS

Our calculations on the hybrid graphene/g-C₃N₄ complex are performed using the plane-wave basis Vienna Ab-initio Simulation Package (VASP) code.^{31,32} An all-electron description, the projector-augmented wave method is used to describe the electron-ion interaction.^{33,34} The state-of-the-art hybrid functional (HSE06) is used for all calculations. A damped van der Waals correction based on Grimme's scheme³⁰ is also incorporated to better describe the nonbonding interaction between graphene and g-C₃N₄ monolayer. The vacuum space in the third dimension (*Z*) is 15 Å, which is enough to separate the interaction between periodic images. A Monkhorst pack mesh of *K* points³⁵ 5 × 5 × 1 and 11 × 11 × 1 points is used, respectively, to sample the two-dimensional Brillouin zone for geometry optimization and calculating the density of states. More than 50 *K* points along each high-symmetry line in the Brillouin zone are used to obtain the accurate band structure. The cutoff energies for plane waves are chosen to be 500 eV, and the convergence tolerance of force on each atom during structure relaxation was set at 0.005 eV/Å.

To calculate the optical properties of graphene/g-C₃N₄ nanocomposite, the frequency-dependent dielectric matrix is calculated using the HSE06 functional and expanding over a 13 × 13 × 1 *K*-point

mesh. The imaginary part is determined by a summation over empty states using the equation³⁶

$$\epsilon''_{\alpha\beta}(\omega) = \frac{4\pi^2 e^2}{\Omega} \lim_{q \rightarrow 0} \frac{1}{q} \sum_{c,v,k} 2\omega_k \delta(\epsilon_{ck} - \epsilon_{vk} - \omega) \times \langle \mu_{ck+e_{\alpha q}} | \mu_{vk} \rangle \langle \mu_{ck+e_{\alpha q}} | \mu_{vk} \rangle^* \quad (1)$$

where the indices *c* and *v* represent conduction and valence band states, respectively, and μ_{ck} refers to the cell periodic part of the orbitals at the *k* point. A large number of empty conduction band states (three times more than the number of valence band) are included for the summation in eq 1.

RESULTS AND DISCUSSIONS

Our g-C₃N₄ model is based on the experimentally well-characterized structure.^{25,26} The lattice constants of g-C₃N₄ and graphene are calculated to be 2.47 and 7.08 Å, respectively, in good agreement with previous studies.³⁷ First, the geometry and electronic structure for the separate graphene and g-C₃N₄ monolayers were calculated, respectively. Figure 1a and 1b

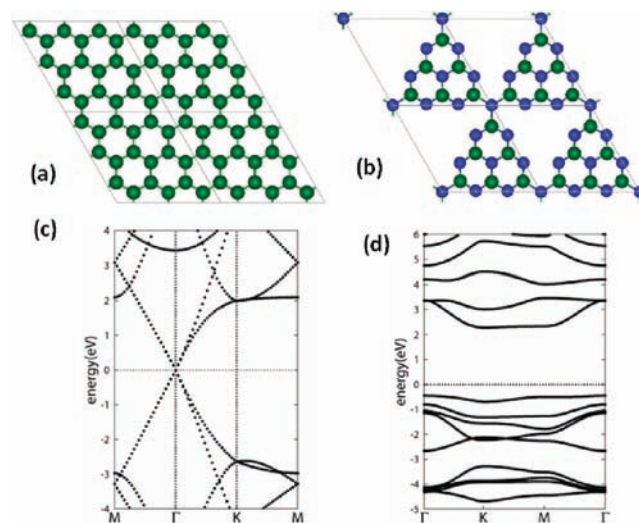


Figure 1. Optimized geometry for a graphene (a) and graphitic carbon nitride (g-C₃N₄) monolayer (b). Band dispersions calculated by the HSE06 functional for graphene (c) and g-C₃N₄ (d). Green and blue spheres represent the C and N atoms, respectively. Note in c that the graphene *K* point in the primitive unit cell is mapped onto the Γ point of the 3 × 3 supercell.

presents their optimized geometry, and Figure 1c and 1d depicts their corresponding band structures calculated at the HSE06 level. It should be noted that the Dirac cone at the *K* point in the graphene primitive unit cell maps onto the Γ point of the 3 × 3 supercell.³⁸ As shown in Figure 1c, the gapless characteristic can be retained in a 3 × 3 graphene superlattice. In contrast to graphene, which is gapless, the band gap of g-C₃N₄ is calculated to be 2.73 eV, consistent with the experimental value.²⁵ Note that this is significantly larger than the value of 1.12 eV by standard DFT based on the generalized gradient approximation.²⁵ Such a difference clearly points to the importance of using the hybrid functional over semilocal DFT in order to obtain an accurate band gap.

In order to simulate the hybrid graphene/g-C₃N₄ nanocomposite, a 3 × 3 graphene supercell is used to match the 1 × 1 g-C₃N₄ unit cell with a small 1.5% strain in graphene. It is worth noting that such a sandwiched interface model is the

most reasonable. In fact, a recent experiment has precisely demonstrated that graphene is intercalated into the g-C₃N₄ layer, and the interaction between graphene and g-C₃N₄ is of π - π type.²⁶ Figure 2a and 2b, respectively, presents a top and

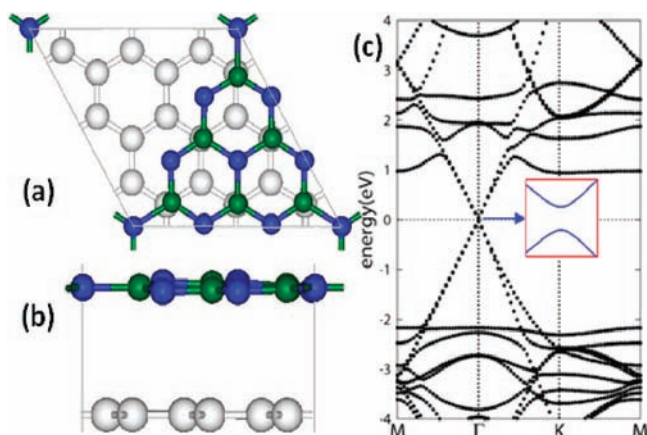


Figure 2. Optimized graphene/g-C₃N₄ interface in a (a) top view and (b) side view. (c) Calculated band structure by the HSE06 functional for graphene supported on g-C₃N₄. (Inset) Magnification of the bands at the Γ point (graphene fold K point). Note, the band gap opening. White, green, and blue balls represent C atoms on graphene and C and N atoms on a g-C₃N₄ monolayer, respectively.

side view of the fully relaxed geometries for hybrid graphene/g-C₃N₄ complex. The equilibrium distance between the graphene layer and the g-C₃N₄ monolayer is calculated to be 3.03 Å. The interface adhesion energy was obtained according to the following equation

$$E_{\text{ad}} = E_{\text{comb}} - E_{\text{graphene}} - E_{\text{g-C}_3\text{N}_4} \quad (2)$$

where E_{comb} , E_{graphene} , and $E_{\text{g-C}_3\text{N}_4}$ represent the total energy of the relaxed hybrid graphene/g-C₃N₄ complex, the pure graphene sheet, and a g-C₃N₄ monolayer, respectively. The interface binding energy is as high as -0.85 eV for the entire model interface, which indicates a very high stability and the π - π stacking interaction as observed by the experiment.²⁶ We should note that the equilibrium distance (adhesion energy) is significantly larger (lower) when one does not consider any long-range dispersion correction. As such it is clear that incorporation of this nonbond interaction³⁰ is extremely important for accurately describing the geometry between the graphene and the g-C₃N₄ monolayers.

The band structure for the hybrid graphene/g-C₃N₄ complex, calculated using the hybrid functional, is shown in Figure 2c. The Dirac cone can still be seen clearly at the Γ point, but closer examination reveals a 70 meV band gap opening as shown in the enlarged inset around the Γ point (see Figure 2c). In order to understand the origin of such a band gap opening, the electrostatic potential difference between the local potential of the hybrid graphene/g-C₃N₄ nanocomposite and that of isolated graphene and g-C₃N₄ monolayers was calculated (see Figure S2 in the Supporting Information). We find that the g-C₃N₄ substrate generates inhomogeneities in the graphene electrostatic potential over the graphene layer. This changes the potential periodicity and therefore disrupts the degeneracy of the π and π^* bands at the Γ point, leading to the band gap opening.

Since the absence of a band gap is a significant hurdle in construction of graphene-based FET, our results make the

hybrid graphene/g-C₃N₄ composite promising as an electronic material. Note that in a hypothetical graphene/g-C₃N₄ based FET the source and drain electrodes should be connected directly to graphene while the g-C₃N₄ monolayer underneath may actually act as a backgate to precisely control the current on-off ratio. Most importantly, the 2-D planar structure of g-C₃N₄ is free of dangling bonds and will provide an ideal substrate for graphene to sit on. Furthermore, a 70 meV band gap is significantly larger than the room-temperature thermal energy ($K_{\text{B}}T$). This gives us hope that the current on/off ratio achievable for the graphene/g-C₃N₄ composite may be larger than that of a freestanding graphene layer. Remarkably, the curvature of band dispersion around the Dirac point of the graphene/g-C₃N₄ composite is very similar to that of graphene (see Figures 1c and 2c). Thus, the effective electron mass and hence the charge mobility is not significantly affected by the g-C₃N₄ support. It is important to note here that such graphene/g-C₃N₄ nanocomposite has been already fabricated experimentally,^{26,28} suggesting that such a hypothetical device may be realizable in the near future.

Having studied the electronic structure of the hybrid graphene/g-C₃N₄ architecture, it is now necessary to explore the electron coupling at the graphene/g-C₃N₄ interface, as this is responsible for the gap opening in the g-C₃N₄-supported graphene. In order to characterize the interfacial electronic structure, three-dimensional charge density difference plots are constructed by subtracting the calculated electronic charge of the hybrid graphene/g-C₃N₄ nanocomposite from that of the independent graphene and g-C₃N₄ monolayers as shown in Figure 3a (a top view) and 3b (a side view). From the figures we can clearly see that the charge density is redistributed by forming triangular-shaped electron-rich and hole-rich regions, i.e., an electron-hole puddle (see a large electron-hole

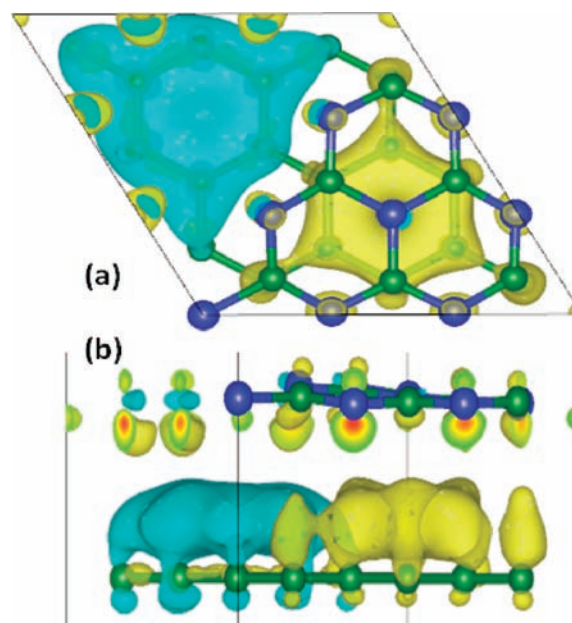


Figure 3. Charge transfer at the graphene/g-C₃N₄ interface: (a) top and (b) side view of the three-dimensional charge density difference plots. Green and blue balls represent C and N atoms, respectively. Yellow and light blue isosurfaces represent, respectively, charge accumulation and depletion in the space with respect to isolated graphene and g-C₃N₄. Note the triangular-shaped electron-hole puddle. The isovalue chosen to plot the isosurfaces is 0.002 e/Å³.

in a large super cell in the Supporting Information) within the graphene layer. Here, formation of the electron–hole puddle is understood as due to the inhomogeneous planar $g\text{-C}_3\text{N}_4$ substrate that drives the interlayer charge transfer from graphene to $g\text{-C}_3\text{N}_4$. Note that this is in contrast to the electron–hole puddle forming in graphene deposited over a SiO_2 substrate, where charged impurities in the substrate play a major role.³⁹ Additionally, it is worth noting that a similar charge transfer has been also demonstrated recently at hybrid graphene/titania interface.⁴⁰ At this point we note that $g\text{-C}_3\text{N}_4$ has been already reported to be a very good metal-free catalyst for oxygen reduction in the proton exchange membrane fuel cells.⁴¹ However, its performances are strongly limited by its low conductivity of $g\text{-C}_3\text{N}_4$. Charge transfer at the graphene/ $g\text{-C}_3\text{N}_4$ interface as predicted here could be expected to significantly enhance the electron conductivity in a $g\text{-C}_3\text{N}_4$ layer.

In order to confirm this hypothesis, the density of state projected onto a $g\text{-C}_3\text{N}_4$ layer in the hybrid graphene/ $g\text{-C}_3\text{N}_4$ complex was calculated (see Figure S3 in the Supporting Information). When compared to the total density of state for an isolated $g\text{-C}_3\text{N}_4$ layer, we notice that new states are induced in the band gap, i.e., the $g\text{-C}_3\text{N}_4$ layer becomes slightly n-doped. This is attributed to electron coupling at the graphene/ $g\text{-C}_3\text{N}_4$ interface. Importantly, our most recent joint experimental and theoretical study has provided indirect evidence for the tremendous oxygen reduction activity in a porous-carbon-supported $g\text{-C}_3\text{N}_4$ material due to the enhanced conductivity.⁴²

As just discussed, the photoabsorption efficiency in $g\text{-C}_3\text{N}_4$ is low due to the lack of visible light response; thus, the material performance in producing hydrogen from water-splitting remains poor.²⁵ Figure 4a shows the HSE06-calculated imaginary part of the dielectric function for a $g\text{-C}_3\text{N}_4$ monolayer. We found that hybrid functional methods can accurately reproduce the experimentally observed optical absorption spectrum.²⁵ Clearly, pure $g\text{-C}_3\text{N}_4$ can only harvest ultraviolet light, and its optical absorption has to be greatly improved in order to move $g\text{-C}_3\text{N}_4$ toward realistic applications in photocatalysis. It is well known that graphene possesses unique optical properties.⁴³ Here, the strong electron coupling demonstrated at the graphene/ $g\text{-C}_3\text{N}_4$ interface may induce a new optical transition. As shown in the band structure of the hybrid graphene/ $g\text{-C}_3\text{N}_4$ complex (Figure 3c), electrons can now be directly excited from the valence band of graphene to the conduction band of $g\text{-C}_3\text{N}_4$. Our most recent work on a hybrid graphene/titania complex has clearly demonstrated that such a mechanism is active in enhancing the visible light response of the complex.⁴⁰ As such the hybrid graphene/ $g\text{-C}_3\text{N}_4$ compound is expected to display an enhanced optical activity in the visible region compared to that of a pure $g\text{-C}_3\text{N}_4$ layer.

In order to examine this effect, the imaginary part of the dielectric function for the hybrid graphene/ $g\text{-C}_3\text{N}_4$ nanocomposite is also calculated and shown in Figure 4b. Remarkably, the absorption spectrum of such a hybrid complex has been significantly expanded from UV light into the visible, indicating that the hybrid graphene/ $g\text{-C}_3\text{N}_4$ nanocomposite could harvest a broad range of visible light efficiently, i.e., it can potentially lead to an enhanced photocatalytic activity. It should be noted that the enhanced visible light response is consistent with the most recent experimental observation at NIMS in Japan.²⁶ Here we should remark that a large number of k points are needed for an accurate calculation of the optical properties

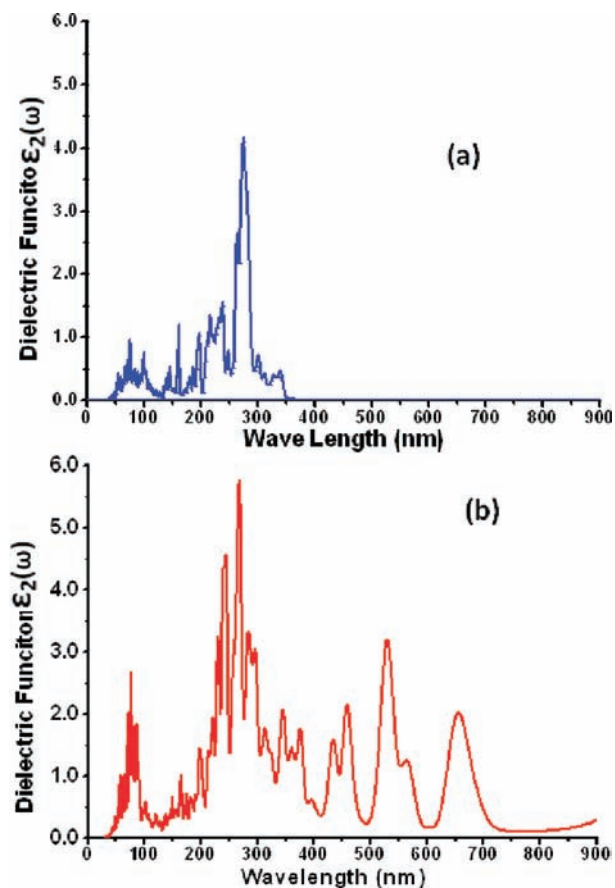


Figure 4. (a) Calculated imaginary part of the dielectric function (in-plane polarization) for a pure $g\text{-C}_3\text{N}_4$ monolayer and (b) hybrid graphene/ $g\text{-C}_3\text{N}_4$ complex.

but that such a large sampling is as yet unreachable when using a hybrid functional for our interface model. However, the implications of the above theoretical analysis on the enhanced visible light response, based on a $13 \times 13 \times 1$ k -point grid, are expected to be robust, and they have been recently demonstrated experimentally.²⁶ Finally, it is important to note that the broadening of the absorption spectrum to the visible region demonstrated here does not necessarily imply an enhancement of the photocatalytic activity. Further direct simulations and experimental measurements of photocatalysis are then needed. However, a good hint comes from a recent work on the hybrid graphene/ $g\text{-C}_3\text{N}_4$ nanocomposite, which indeed shows very high photocatalytic activity for water splitting.²⁸

CONCLUSIONS

In summary, we investigated the graphene/ $g\text{-C}_3\text{N}_4$ interface by state-of-the-art hybrid functional DFT methods incorporating long-range dispersion corrections. Our calculations could precisely reproduce the experimentally observed band gap and optical absorption spectrum for $g\text{-C}_3\text{N}_4$ material. We revealed for the first time a strong electronic coupling at the graphene/ $g\text{-C}_3\text{N}_4$ interface. A band gap (around 70 meV) opens by forming an electron–hole puddle in a $g\text{-C}_3\text{N}_4$ -supported graphene monolayer, and this may overcome one of the main hurdles of using graphene as an electronic material, namely, the lack of an intrinsic band gap. Furthermore, the charge transfer at the graphene/ $g\text{-C}_3\text{N}_4$ interface enhances the

electron conductivity of $g\text{-C}_3\text{N}_4$, potentially facilitating oxygen reduction reaction compared to that in a pure $g\text{-C}_3\text{N}_4$ material. Additionally, the hybrid graphene/ $g\text{-C}_3\text{N}_4$ complex displays an enhanced optical absorption behavior in the visible light region, promising novel applications in photocatalysis and photovoltaic devices.

■ ASSOCIATED CONTENT

■ Supporting Information

Geometry coordinates and energies for a $g\text{-C}_3\text{N}_4$ layer and the hybrid graphene/ $g\text{-C}_3\text{N}_4$ interface complex, a large electron–hole puddle in a large super cell, and projected density of state onto $g\text{-C}_3\text{N}_4$ layer in the combined graphene/ $g\text{-C}_3\text{N}_4$ nanocomposite. This material is available free of charge via the Internet at <http://pubs.acs.org>.

■ AUTHOR INFORMATION

Corresponding Author

E-mail: a.du@uq.edu.au

Notes

The authors declare no competing financial interest.

■ ACKNOWLEDGMENTS

We acknowledge generous grants of high-performance computer time from the AIBN cluster computing facility at The University of Queensland and the Australian Research Council (LIEF grant LE0882357: A Computational Facility for Multiscale Modeling in Computational Bio and Nanotechnology), Queensland Cyber Infrastructure Foundation (QCIF), and the Australian Partnership for Advanced Computing National Facility. A.D. also greatly appreciates the QEII Fellowship and financial support of the Australian Research Council under Discovery Project (DP110101239). S.C.S. acknowledges support from the Center for Nanophase Materials Sciences, which is sponsored at the Oak Ridge National Laboratory by the Scientific User Facilities Division, U.S. Department of Energy. S.S. thanks the Science Foundation of Ireland (Grant no. 07/IN.1/1945) and CRANN for financial support.

■ REFERENCES

- (1) Novoselov, K. S.; Geim, A. K.; Morozov, S. V.; Jiang, D.; Zhang, Y.; Dubonos, S. V.; Grigorieva, I. V.; Firsob, A. A. *Science* **2004**, *306*, 666.
- (2) Geim, A. K.; Novoselov, K. S. *Nat. Mater.* **2007**, *6*, 183.
- (3) Falko, V. *Nat. Phys.* **2007**, *3*, 151.
- (4) Son, Y. W.; Cohen, M. L.; Louie, S. G. *Nature* **2006**, *444*, 347.
- (5) Novoselov, K. S.; Jiang, D.; Schedin, F.; Booth, T. J.; Khotkevich, W.; Morozov, S. V.; Geim, A. K. *Proc. Nat. Acad. Sci., U.S.A.* **2005**, *102*, 10451.
- (6) Brumfiel, G. *Nature* **2009**, *458*, 390.
- (7) Du, A. J.; Smith, S. C. *J. Phys. Chem. Lett.* **2011**, *2*, 73.
- (8) Kosynkin, D. V.; Higginbotham, A. L.; Sinitskii, A.; Lomeda, J. R.; Dimiev, A.; Price, B. K.; Tour, J. M. *Nature* **2009**, *458*, 872.
- (9) Jiao, L.; Zhang, L.; Wang, X.; Diankov, G.; Dai, H. *Nature* **2009**, *458*, 877.
- (10) Guinea, F.; Katsnelson, M. I.; Gerim, A. *Nat. Phys.* **2010**, *6*, 30.
- (11) Ni, Z. H.; Yu, T.; Lu, Y. H.; Wang, Y. Y.; Feng, Y. P.; Shen, Z. X. *ACS Nano* **2008**, *2*, 2301.
- (12) Balog, R.; Jørgensen, B.; Nilsson, L.; Andersen, M.; Rienks, E.; Bianchi, M.; Fanetti, M.; Lægsgaard, E.; Baraldi, A.; Lizzit, S.; Slijivancanin, Z.; Besenbacher, F.; Hammer, B.; Pedersen, T. G.; Hofmann, P.; Homekaer, L. *Nat. Mater.* **2010**, *9*, 315–319.

- (13) Du, A. J.; Zhu, Z. H.; Smith, S. C. *J. Am. Chem. Soc.* **2010**, *132*, 2876.
- (14) Zhou, S. Y.; Gweon, G. H.; Fedorov, A. V.; First, P. N.; De Heer, W. A.; Lee, D. H.; Guinea, F.; Neto, A. H. C.; Lanzara, A. *Nat. Mater.* **2007**, *6*, 770.
- (15) Zhang, W. J.; Lin, C. T.; Liu, K. K.; Tite, T.; Su, C. Y.; Chang, C. H.; Lee, Y. H.; Chu, C. W.; Wei, K. H.; Kuo, J. L.; Li, L. J. *ACS Nano* **2011**, *9*, 7517.
- (16) Wang, F.; Zhang, Y. B.; Tian, C. S.; Girit, C.; Zettl, A.; Crommie, M.; Shen, Y. R. *Science* **2008**, *320*, 206.
- (17) Zhang, Y. B.; Tang, T. T.; Girit, C.; Hao, Z.; Martin, M. C.; Zettl, A.; Crommie, M. F.; Shen, Y. R.; Wang, F. *Nature* **2009**, *459*, 820.
- (18) Decker, R.; Wang, Y.; Brar, V. W.; Regan, W.; Tsai, H. Z.; Wu, Q.; Gannett, W.; Zettl, A.; Crommie, M. F. *Nano Lett.* **2011**, *11*, 2291.
- (19) Liao, L.; Lin, Y. C.; Bao, M. Q.; Cheng, R.; Bai, J. W.; Liu, Y.; Qu, Y. Q.; Wang, K. L.; Huang, Y.; Duan, X. F. *Nature* **2010**, *467*, 305.
- (20) Lin, Y. M.; Dimitrakopoulos, C.; Jenkins, K. A.; Farmer, D. B.; Chiu, H. Y.; Grill, A.; Avouris, Ph. *Science* **2010**, *327*, 662.
- (21) Chen, J. H.; Jiang, C.; Xiao, S.; Ishigami, M.; Fuhre, M. S. *Nat. Nanotechnol.* **2008**, *3*, 206.
- (22) Ponomarenko, L. A.; Yang, R.; Mohiuddin, T. M.; Katsnelson, M. I.; Novoselov, K. S.; Morozov, S. V.; Zhukov, A. A.; Schedin, F.; Hill, E. W.; Geim, A. K. *Phys. Rev. Lett.* **2009**, *102*, 206603.
- (23) Xue, J. M.; Sanchez-Yamagishi, J.; Bulmash, D.; Jacquod, P.; Deshpande, A.; Watanabe, K.; Taniguchi, T.; Jarillo-Herrero, P.; LeRoy, B. J. *Nat. Mater.* **2011**, *10*, 282–285.
- (24) Kharache, N.; Nayak, S. K. *Nano Lett.* **2011**, *11*, 5274–5278.
- (25) Wang, X. C.; Maeda, K.; Thomas, A.; Takanabe, K.; Xin, G.; Carisson, J. M.; Domen, K.; Antonietti, M. *Nat. Mater.* **2009**, *8*, 76.
- (26) Zhang, Y. J.; Mori, T.; Niu, L.; Ye, J. H. *Energy Environ. Sci.* **2011**, *4*, 4517.
- (27) Zhang, Y. J.; Mori, T.; Ye, J. H.; Antonietti, M. *J. Am. Chem. Soc.* **2010**, *132*, 6294.
- (28) Xiang, Q. J.; Yu, J. G.; Jaroniec, M. *J. Phys. Chem. C* **2011**, *115*, 7355.
- (29) Heyd, J.; Scuseria, G. E.; Ernzerhof, M. *J. Chem. Phys.* **2006**, *124*, 219906.
- (30) Grimme, S. *J. Comput. Chem.* **2006**, *27*, 1787.
- (31) Kresse, G.; Furthmüller, J. *Comput. Mater. Sci.* **1996**, *6*, 15.
- (32) Kresse, G.; Furthmüller, J. *Phys. Rev. B* **1996**, *54*, 11169.
- (33) Blochl, P. E. *Phys. Rev. B* **1994**, *50*, 17953.
- (34) Kresse, G.; Joubert, D. *Phys. Rev. B* **1999**, *59*, 1758.
- (35) Monkhorst, H. J.; Pack, J. D. *Phys. Rev. B* **1976**, *13*, 5188.
- (36) Gajdos, M.; Hummer, K.; Kresse, G.; Furthmüller, J.; Bechstedt, F. *Phys. Rev. B* **2006**, *73*, 045112.
- (37) Deifallah, M.; McMillan, P. F.; Cora, F. *J. Phys. Chem. C* **2008**, *112*, 5447.
- (38) Guinea, F.; Low, T. *Philos. Trans. R. Soc. London, Ser. A* **2010**, *368*, 5391.
- (39) Martin, J.; Akerman, N.; Ulbricht, G.; Lohmann, T.; Smet, J. H.; von Klitzing, K.; Yacoby, A. *Nat. Phys.* **2008**, *4*, 144.
- (40) Du, A. J.; Ng, Y. H.; Bell, N. J.; Zhu, Z. H.; Amal, R.; Smith, S. C. *J. Phys. Chem. Lett.* **2011**, *2*, 894.
- (41) Sun, Y. Q.; Li, C.; Xu, Y. X.; Bai, H.; Yao, Z. Y.; Shi, G. Q. *Chem. Commun.* **2010**, *46*, 4740.
- (42) Zheng, Y.; Jiao, Y.; Chen, J.; Liu, J.; Liang, J.; Du, A. J.; Zhang, W. M.; Zhu, Z. H.; Smith, S. C.; Jaroniec, M.; Lu, G. Q.; Qiao, S. Z. *J. Am. Chem. Soc.* **2011**, *133*, 20116.
- (43) Bonaccorso, F.; Sun, Z.; Hasan, T.; Ferrari, A. C. *Nat. Photonics* **2010**, *4*, 611.